Journal of Information Processing Vol.25 No.4 1–10 (Oct. 2017)

[DOI: 10.2197/ipsjjip.25.1]

Regular Paper

Folded Structures Satisfying Multiple Conditions

Erik D. Demaine[1,a)] Jason S. Ku[1,b)]

Received: November 7, 2016, Accepted: May 16, 2017

Abstract:
Isometries always exists to fold a paper to match a non-expansive folding of its boundary. However, there is little known about designing crease patterns that satisfy multiple constraints at the same time. In this paper, we analyze crease patterns that can fold to multiple prescribed folded boundaries, as well as flat-foldable states, such that every crease in the crease pattern is finitely folded in each folding. Additionally, we show how to layout simpler units in a grid to approximate triangulated surfaces.

Keywords: Computational geometry, computational origami, boundary conditions

1. Introduction

The study of folding is a rich and burgeoning mathematical, computational, and engineering field inspired by the ancient Japanese art of paper folding.[*1] In recent years, many algorithms and software have been produced to aid the design of complex families of folded structures. Lang introduced Tree Theory to design uniaxial origami bases [2]; Tachi's work on Origamizer [4] and generalized parameterized models [3] facilitate the design of three dimensional folded structures. Ku et al. proposed a folded structure design paradigm starting from a prescribed boundary condition on a paper [1].

These design algorithms and others focus on producing crease patterns that fold to single designed states. However, there is little research in designing crease patterns that satisfy multiple constraints across multiple folded states. In this paper, we explore techniques to design crease patterns that can fold to multiple prescribed folded boundaries, as well as flat-foldable states, such that every crease in the crease pattern is finitely folded in each folding. Additionally, we show how to combine simpler units into a grid to approximate triangulated surfaces. Throughout, we will only argue isometric existence of constructed developable geometry and ignore possible material self-intersection. We leave rigorous arguments guaranteeing non-self-intersection to future work.

We restrict much of our analysis to quadrilateral papers whose boundaries only fold at corners of the paper, i.e. boundaries that are cyclic four bar linkages. While this model is simple and limited, it is also surprisingly powerful. Such a linkage has two degrees of freedom that can be parameterized by specifying the distances between non-adjacent vertices. We show that not only do isometries exist that fold to a given boundary condition, but there exist both satisfying isometries that are also flat-foldable, and single crease patterns that satisfy two different boundary conditions using the same set of creases. We hope this work can lead to a broader exploration of multi-degree of freedom systems, and the design of crease patterns with a large number of functional folded states. In particular, our results have direct application to re-configurable mechanical systems and programmable materials.

[1] MIT Computer Science and Artificial Intelligence Laboratory, 32 Vassar Street, Cambridge, MA 02139, USA
[a)] edemaine@mit.edu
[b)] jasonku@mit.edu

[*1] The latest 6OSME conference (Tokyo, 2014) embodies all of these directions. Recent mechanical engineering effort have been the topic of an NSF program (ODISSEI) and several sessions at ASME, IASS, and JMA conferences.

2. Boundary Conditions

As shown in [1], given a non-expansive folding of the boundary of a paper folded at finitely many boundary points (the *boundary condition*), there always exists an isometric folding of the paper that matches the boundary condition. In fact, when the solution is not unique, an infinite number of isometries exist. The result provides a construction for such a solution in polynomial time. In this section we will analyze the solution space of all possible crease patterns for some special cases of paper, and restrictions on the number of allowed interior crease pattern vertices.

As there are generally an infinite number of crease patterns that fold to a generic boundary condition, it is useful to study minimal satisfying solutions: for example, solutions that require the fewest number of interior vertices. A direct corollary from the construction outlined in [1] is that, for quadrilateral paper whose boundary acts like a cyclic four bar linkage, a single vertex crease pattern always exists that satisfies any non-expansive boundary condition. One can specify such a crease pattern by giving the location of the single interior vertex, and then drawing from it a crease to each boundary vertex.

By solving the isometric distance constraints between the unfolded and folded configuration of a folded quadrilateral bound-

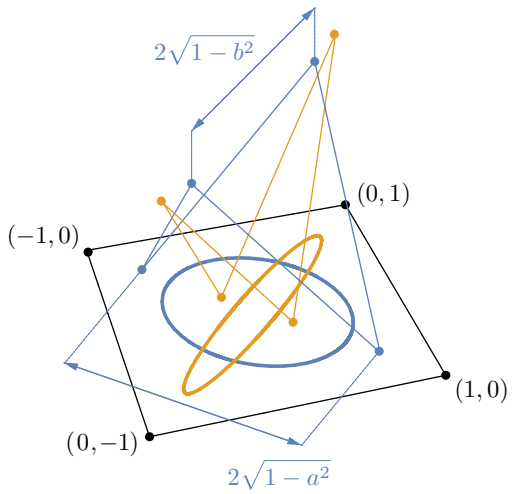

Fig. 1 Ellipses corresponding to the space of possible single vertex locations corresponding to crease patterns that fold to two different boundary conditions.

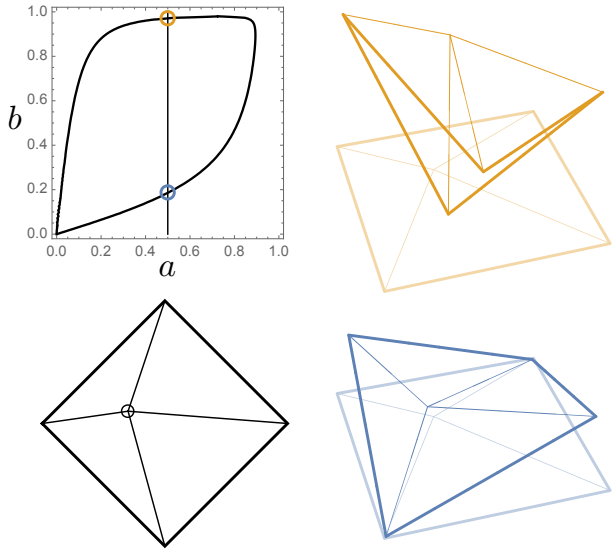

Fig. 2 The state space of a single vertex crease pattern, plotting a vs. b, and two folded states for a single value of a. The orange state has a high value of b so the top and bottom points are close together. The blue state has a low value of b so the bottom points are far apart.

ary, one can show that the locus of possible 2D single vertex locations on the paper satisfying a folding of its boundary is an ellipse; see the appendix for a derivation. The equation of this locus in general is quite complicated. However, in the case of kite quadrilaterals, the locus is an ellipse axis aligned with the diagonals, and for squares the ellipse is centered. We will focus our analysis on squares, but any quadrilateral may be analyzed using a similar approach. Let the corners of the square be $(-1,0)$, $(0,1)$, $(1,0)$ and $(0,-1)$. We parameterize the folding of the square boundary by the distances between the two diagonals, distance $2\sqrt{1-a^2}$ along the x axis and distance $2\sqrt{1-b^2}$ along the y axis; choosing this parameterization simplifies the equations later on. Using this parameterization, the equation of the ellipse of crease pattern vertices satisfying the boundary condition (a,b) is as follows:

$$\frac{x^2}{a^2(1-b^2)} + \frac{y^2}{b^2(1-a^2)} = a^2 + b^2. \qquad (1)$$

Figure 1 shows ellipses corresponding to two different boundary conditions. Since the ellipse is centered at the origin, it must cross both the x and y axes twice, except in the degenerate cases where the ellipse becomes a line or a point, i.e. when a or b equal 1 or 0. When both a and b equal 0, the square is flat in the folding and any point on the square will be a solution. When exactly one of a or b equals 0, the diagonal is exactly the same length in the folding as in the boundary folding and any point on the diagonal will be a solution. When a or b equals 1, a line segment of solutions exist. When both a and b equal 1, the only solution is the center of the paper.

If we choose a crease pattern by fixing (x,y), Equation 1 defines a quartic function on a and b, prescribing the one degree of freedom mechanism of the crease pattern. Figure 2 shows a plot of this state space for one such crease pattern. The bottom left corner corresponds to the flat state when $(a,b) = (0,0)$.

3. Flat-Foldability

When designing folded structures, one desirable condition is

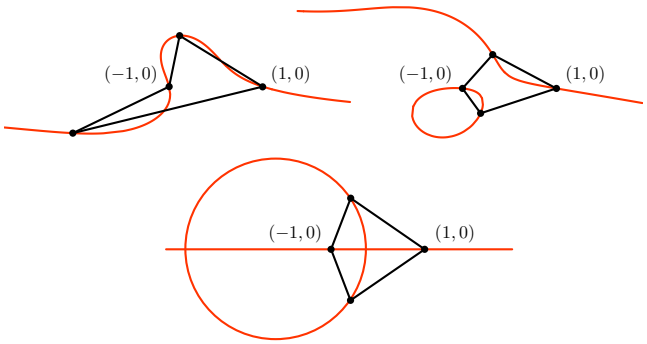

Fig. 3 Locus of flat-foldable single-vertex locations for various generic quadrilaterals: reflex, convex, and kite.

for the crease pattern to be *flat-foldable*, i.e. the crease pattern can fold along each crease and fold flat. This condition is often desirable to achieve a large range of motion and a compact collapsed state.

Theorem 1. *Given a four cornered paper, there exists a single vertex crease pattern folding through each corner of the paper that folds flat.*

Proof. A single degree-four vertex in a flat-foldable crease pattern must obey Kawasaki's theorem, the sum of opposite angles sum to π. In fact, satisfying Kawasaki's theorem is both necessary and sufficient for flat-foldability. From this condition, one can derive a condition on possible positions (x,y) of the single vertex. We can parameterize any simple quadrilateral with cyclically ordered points $(-1,0)$, (x_1,y_1), $(1,0)$, and (x_2,y_2), where y_1 is positive, y_2 is negative, and the line from $(-1,0)$ to $(1,0)$ is a visible diagonal. With this parameterization, the condition on the location of a flat-foldable vertex is given by the following cubic equation:

$$x(y_1+y_2)(x^2+y^2-1)-y(x_1+x_2)(x^2+y^2+1)+ (x_1y_2+x_2y_1)(y^2-x^2+1)+2xy(1+x_1x_2-y_1y_2)=0. \quad (2)$$

Figure 3 shows the locus curve defined by Equation 2 for a few choices of quadrilateral. The curve defined by this equation passes through each corner of the paper, as can be readily verified. However, we must prove that the curve passes through the interior of the paper. It suffices to show that the tangent to the curve at one of the vertices passes between its two adjacent edges. Taking partial derivatives of Equation 2, one can show the tangent to the curve at $(-1,0)$ has the same direction the following vector:

$$v=\left((x_1+1)(x_2+1)-y_1y_2, y_1(x_2+1)+y_2(x_1+1)\right). \quad (3)$$

The edges adjacent to $(-1,0)$ have directions $u=(x_1+1,y_2)$ and $w=(x_2+1,y_2)$ respectively. Taking magnitude of the cross products in the $\hat{z}$ direction out of the plane yields the following relations:

$$(v\times u)\cdot\hat{z}=-((1+x_1)^2+y_1^2)y_2; \quad (4)$$
$$(v\times w)\cdot\hat{z}=-((1+x_2)^2+y_2^2)y_1. \quad (5)$$

Because y_2 is always negative, the first condition is always positive, so the top edge is a left turn from the tangent line. Because y_1 is always positive, the second condition is always negative, so the bottom edge is a right turn from the tangent line. Thus local to $(-1,0)$, the curve must intersect the quadrilateral, completing the proof. □

In the special case of a kite quadrilateral where each edge is adjacent to an edge of the same length, Equation 2 degenerates into a line and circle. This can be shown by imposing the condition $x_1=x_2$ and $y_1=-y_2$. The resulting curve is as follows:

$$y\left(\left(x-\frac{1+x_1^2+y_1^2}{2x_1}\right)^2+y^2+1-\left(\frac{1+x_1^2+y_1^2}{2x_1}\right)^2\right)=0. \quad (6)$$

And for a square, when $x_1=x_2=0$ and $y_1=-y_2=1$, the solution space is simply the two diagonals of the square:

$$xy=0. \quad (7)$$

For a square boundary, because the locus of flat-foldable single vertices comprises the diagonals of the square, and the locus of single vertices folding to any given boundary condition is a centered ellipse, the following theorem follows directly.

Theorem 2. *Given a square of paper and a folding of its boundary folded only at the corners such that opposite corners are contractive under the folding and not folded to the same point, there are exactly four single-vertex flat-foldable crease patterns satisfying the boundary condition.*

4. Two Boundary Conditions

Now we wish to examine crease patterns that can fold to two different boundary conditions at the same time. For simplicity, we examine squares, using the same parameterization as in Section 2.

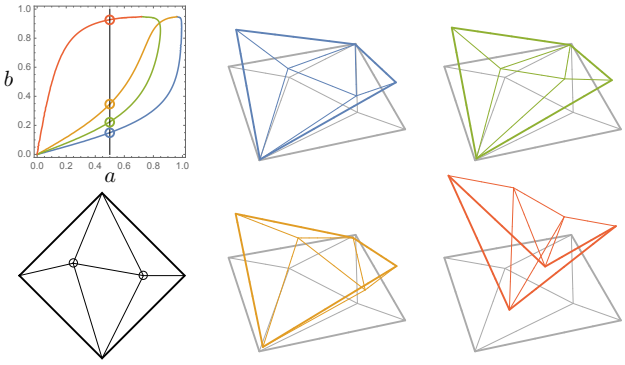

Fig. 4 The state space of a two vertex crease pattern, plotting a vs. b, and four folded states for a single value of a.

4.1 Single Vertex Crease Patterns

Sometimes, we can satisfy two boundary conditions at the same time with a single vertex crease pattern, but this is not always possible.

Theorem 3. *Given a square of paper and two foldings (a_1,b_1), (a_2,b_2) of its boundary folded only at the corners, then if the intervals $[a_1,b_1]$ and $[a_2,b_2]$ overlap, then there exists a single vertex crease pattern that folds exactly to both boundaries.*

Proof. The proof is by construction. The approach will be to calculate the set of possible crease patterns with one interior vertex that folds to each boundary, and show that the two sets have crease patterns in common when the intervals $[a_1,b_1]$ and $[a_2,b_2]$ overlap.

We have already shown that the solution space for each boundary condition is an ellipse given by Equation 1. Given two such ellipses, parameterized by (a_1,b_1) and (a_2,b_2), because the roles of a and b are interchangeable, the ellipses can be made to intersect as long as the smaller major radius is larger than the minor radius of the other. Specifically, the following must hold:

$$\begin{aligned}&\left(\left(1-a_1^2\right)\left(\left(1-b_2^2\right)-\left(1-b_1^2\right)\left(a_2^2+b_2^2\right)\right)-\right.\\&\quad\left.\left(1-a_2^2\right)\left(\left(1-b_1^2\right)-\left(1-b_2^2\right)\left(a_1^2+b_1^2\right)\right)\right)\\&\left(\left(1-b_1^2\right)\left(\left(1-a_2^2\right)-\left(1-a_1^2\right)\left(a_2^2+b_2^2\right)\right)-\right.\\&\quad\left.\left(1-b_2^2\right)\left(\left(1-a_1^2\right)-\left(1-a_2^2\right)\left(a_1^2+b_1^2\right)\right)\right)\le 0.\end{aligned} \quad (8)$$

A simple yet tedious case analysis shows that this equation holds when intervals $[a_1,b_1]$ and $[a_2,b_2]$ overlap. The converse statement is not true as there are points where the intervals do not overlap such that the inequality is still true. Figure 5 depicts the relevant regions of the configuration space over a_1,b_1,a_2,b_2. □

4.2 Two-Vertex Crease Patterns

While single-vertex crease patterns cannot satisfy any two boundary conditions, adding additional interior vertices to the design space for the crease pattern can add flexibility. Figure 4 shows a plot of the boundary state space for a two-vertex crease pattern. The bottom left corner corresponds to the flat state.

Theorem 4. *Given any two nonexpansive boundary foldings of*

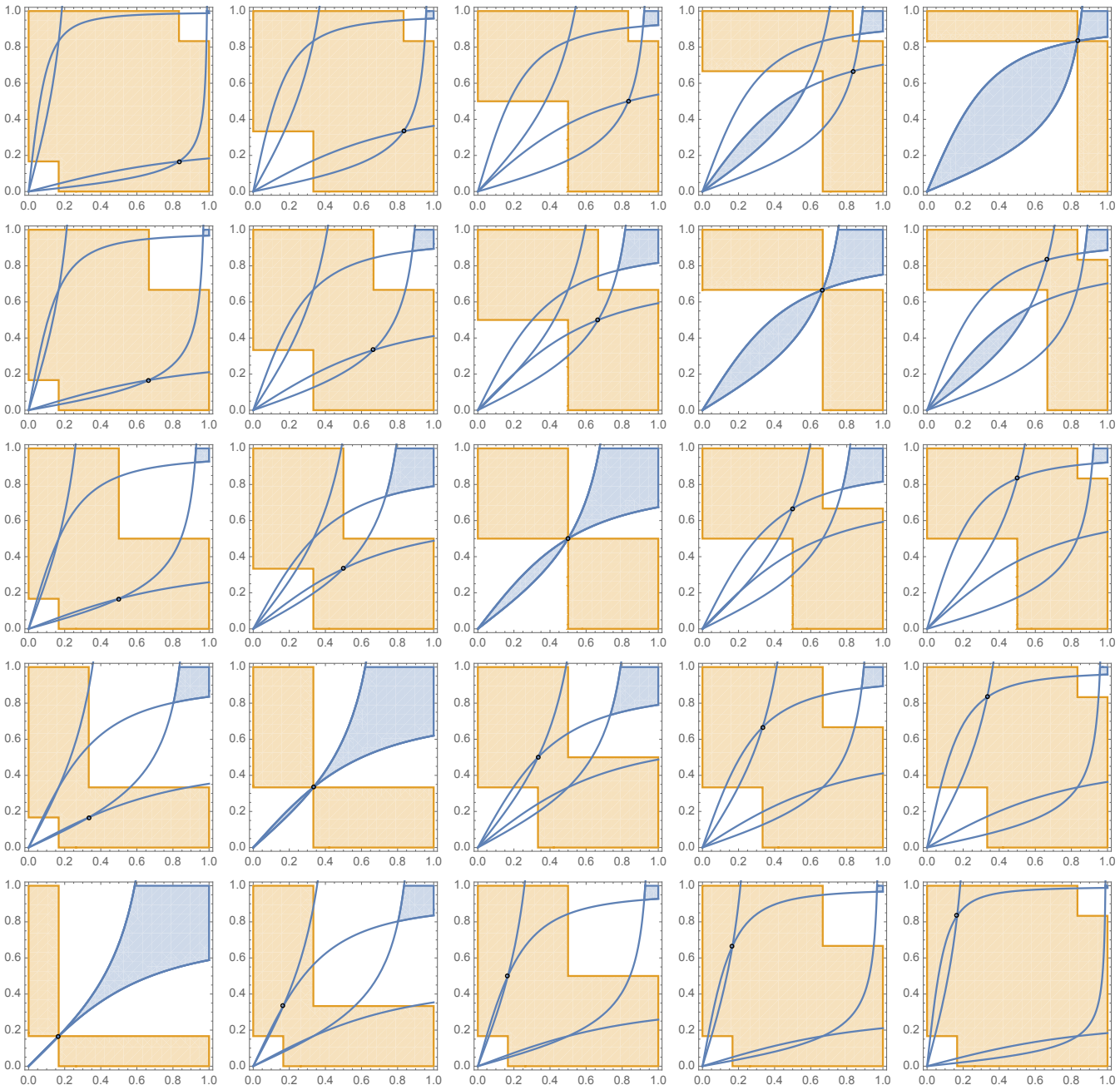

Fig. 5 Plots showing regions where single vertex crease patterns do not exist. For a fixed (a_1, b_1) marked by a black dot, the plot at the corresponding coordinate ranges over possible values of (a_2, b_2). The orange region represents the values of (a_2, b_2) such that the intervals $[a_1, b_1]$ and $[a_2, b_2]$ overlap, as stated in the claim. The blue region indicates the values of (a_2, b_2) that prescribe an ellipse which completely surrounds the ellipse prescribed by (a_1, b_1) or lies completely inside the ellipse prescribed by (a_1, b_1). The white region indicates values not covered by the interval rule of thumb that actually do admit a solution.

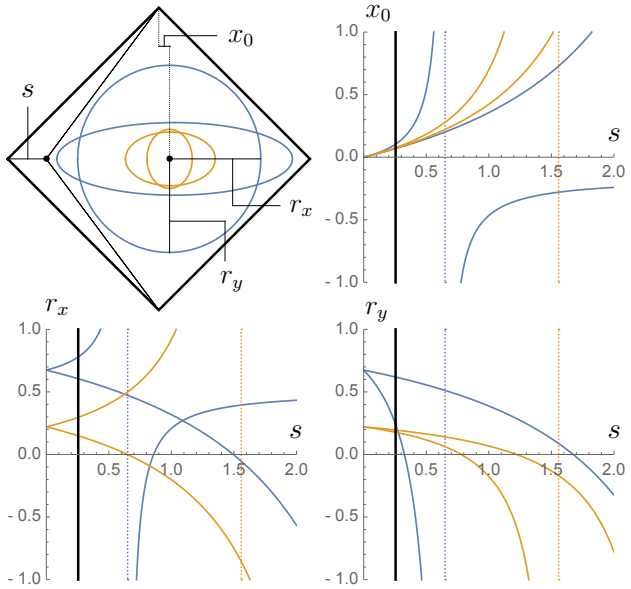

Fig. 6 Graphs of how x_0, r_x, and r_y vary with respect to s for $(a_1, b_1) = (0.3, 0.3)$ (blue) and $(a_2, b_2) = (0.95, 0.95)$ (orange).

a square paper folding at its vertices, there exists a one or two-vertex crease pattern that can fold rigidly to meet both boundary conditions.

Proof. The proof is by construction. The approach will be to calculate a subset of possible crease patterns with two interior vertices that fold to each boundary, and show that the two sets have crease patterns in common.

We will parameterize a subset of two-vertex crease patterns in the special case where one vertex resides on a diagonal. We will let s be the distance between this vertex p and point $(-1, 0)$. Solving the distance constraints on the remaining kite quadrilateral again yields the equation of an ellipse:

$$\frac{(x - x_0)^2}{r_x^2} + \frac{y^2}{r_y^2} - 1 = 0. \tag{9}$$

However, now there are two possible ellipses for each choice of boundary condition: one when the crease from $(-1, 0)$ to p is a valley fold, and one when the crease is a mountain fold. The parameters of the ellipse in each case are given by:

$$x_0 = \frac{sb^2(1 + b^2)}{2(a^2 + b^2)((1 - s) + b^2) \pm 2sb\sqrt{1 - a^2}\sqrt{a^2 + b^2}}; \tag{10}$$

$$r_x = b\sqrt{\frac{1 - a^2}{a^2 + b^2}} - \frac{sb^2(1 - b^2)}{2(a^2 + b^2)((1 - s) + b^2) \pm 2sb\sqrt{1 - a^2}\sqrt{a^2 + b^2}}; \tag{11}$$

$$r_y = a\sqrt{\frac{1 - b^2}{a^2 + b^2}}\left(1 - \frac{sb^2}{(a^2(1 - s) + b^2) \pm b\sqrt{1 - a^2}\sqrt{a^2 + b^2}}\right). \tag{12}$$

Figure 6 shows how x_0, r_x, and r_y vary with respect to s for two prescribed boundary conditions. When $s = 0$, this parameterization reduces Equation 9 to Equation 1. The equations will define an ellipse as long as r_y is not negative, which is true for small enough s. If no single-vertex crease pattern exists, the ellipses corresponding to (a_1, b_1) and (a_2, b_2) do not intersect at $s = 0$.

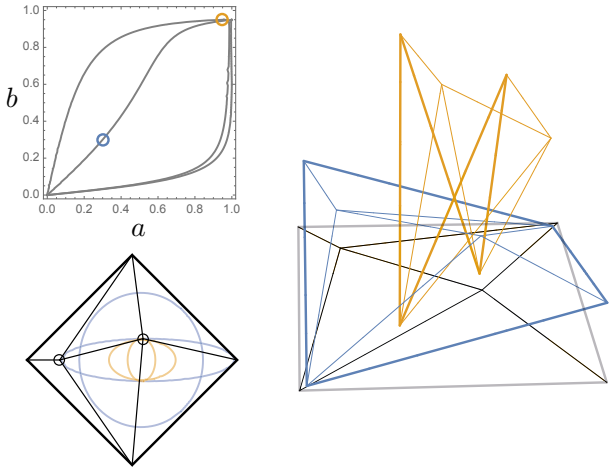

Fig. 7 A crease pattern that satisfies two boundary conditions for $(a_1, b_1) = (0.3, 0.3)$ (blue) and $(a_2, b_2) = (0.95, 0.95)$ (orange), along with the foldings that satisfy the constraints.

That means both r_x and r_y are larger for one ellipse than the other since x_0 is zero. By Theorem 3, without loss of generality we may assume $a_1 > a_2$ and $b_1 > b_2$. We can then solve for s when r_y is zero, specifically:

$$s' = 1 \pm b\sqrt{\frac{1 - a^2}{a^2 + b^2}}. \tag{13}$$

We observe that s' is symmetric about $s = 1$ for any (a, b) when r_y is zero. Since r_y for (a_1, b_1) and (a_2, b_2) are separated from each other when crossing the $s = 0$ axis, and their curves nest inside each other when crossing the $r_y = 0$ axis, then r_y for (a_1, b_1) and r_y for (a_2, b_2) must be equal for some s. If they are equal, their corresponding ellipses must intersect, which corresponds to a two-vertex crease pattern satisfying both boundary conditions. □

Figure 7 shows an example two-vertex crease pattern solution that folds to both boundary conditions, for a condition set that cannot be satisfied using a single-vertex crease pattern.

When looking at the boundary state space for two vertex crease patterns, we observe two loops rather than the one loop we see for single-vertex crease patterns (see Figures 4 and 7). These crease patterns have local single degree of freedom away from the flat state and thus no choice when folding. However, when departing the flat state the two-vertex crease pattern has extra freedom to choose a valid mountain/valley assignment for its creases, which results in two modes of folding through the state space. This flexibility allows for more boundary states to be accessed by folding the same set of creases. As the number of allowed interior vertices increases, it may be possible to densely fill the boundary state space with a single crease pattern. We conjecture that any finite set of boundary conditions on a square paper can be satisfied with a finite crease pattern such that every crease folds by a nonzero amount when satisfying each boundary folding.

5. Approximating Triangulated Surfaces

The previous sections have provided an in-depth study of folded square boundaries folded only through their corners. Because this restriction is simple and the low dimensional boundary

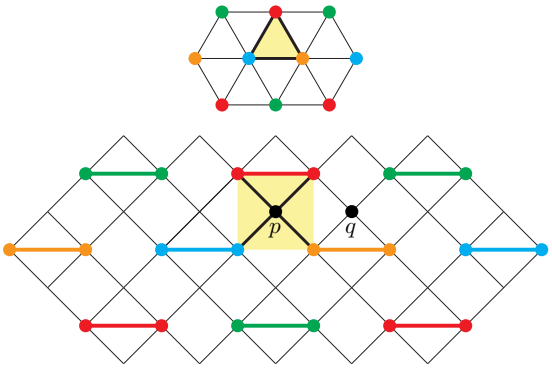

Fig. 8 Square grid to triangulation vertex correspondence for the slowly varying 6-regular construction. Two square grid vertices map onto each triangulated surface vertex. Points p and q are both square grid vertices associated with a face of the triangulation.

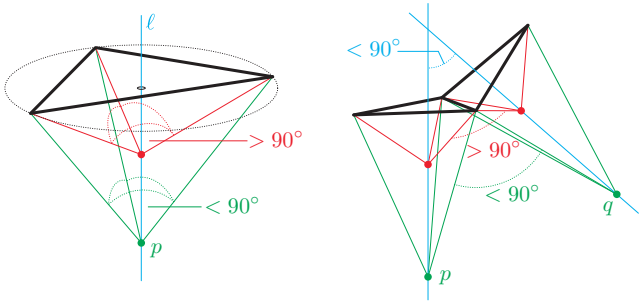

Fig. 9 Angles subtended by square grid edges incident to face vertices [Left] and corner vertices [Right] can be made less than 90° in the mapping by choosing sufficiently large square grid edge length. Red and green coloring correspond to mappings of p and q that have expansive and contractive square boundaries respectively.

state space is relatively easy to control, such units could be used to design more complicated surfaces if we could combine many of them together in an organized way. In this section, we introduce two ways of combining these squares to approximate *6-regular* triangulated orientable surfaces, where each non-boundary vertex of the triangulation is bounded by exactly six triangles.

We call a folded structure an *ε-approximation* of a target polyhedral surface if every point on the approximate surface is at most distance ε from some point of the target surface, and every point on the target surface is at most distance ε from some point on the approximate surface. Thus, an ε-approximation will be the target surface for $\varepsilon = 0$. Again, building off of [1], we only seek to construct isometries and leave the question of self-intersection to future work.

We restrict our study to 6-regular triangulated surfaces because they are topologically equivalent to the equilateral triangular grid that tiles the plane. The approach will be to fold a square grid to the triangle grid, and then shorten edge lengths until the target surface is achieved. We would like to construct these surfaces from square boundaries because, from the previous discussion, non-adjacent vertex distances can be controlled via an engineered crease pattern inside the square. By associating square diagonals with target surface edges, one could hope to control their individual lengths independently.

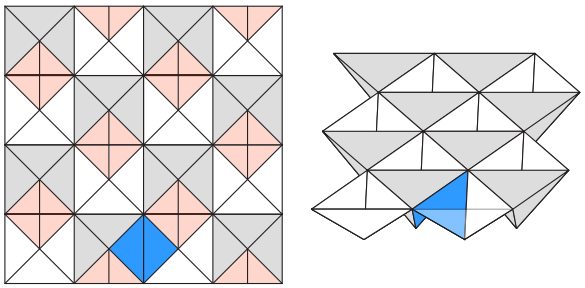

Fig. 10 A folding approximating an equilateral triangular grid.

5.1 Slowly Varying 6-Regular

First, we describe a method to construct ε-approximations to *slowly varying* 6-regular triangulated orientable surfaces, where the angle subtended by any two vertex adjacent face normals is strictly less than 90°. In particular, given such a surface, we construct a one-sided ε-approximation existing only on the 'inner' side, in addition to containing the vertex set of the target surface.

Theorem 5. *Given a slowly varying 6-regular triangulated surface, there exists a folding that is an ε-approximation to the surface for any positive value of ε.*

Proof. We associate a grid of squares with our target triangulated surface as shown in Figure 8. We construct a folding of the square grid that maps two square grid vertices onto a single triangulated surface vertex, while keeping square grid edges uncreased, i.e. only folding at square corners. We calculate the size of the grid needed relative to the geometry of the triangulated surface in order for such an isometry to exist. In this section, we call square grid vertices that map to triangle vertices *corner vertices*, and all other vertices *face vertices*. Note that by construction, there is one face vertex per triangle in the target surface.

Consider the highlighted triangle and its corresponding grid region. We define a folding of the grid by mapping corner vertices onto their associated triangulated surface vertices. In order for a folding to exist from the square grid to the triangulated surface, we must locate the face vertices, e.g. vertex p, to be equidistant to the triangle's three vertices. Then when folded, point p must lie on the line ℓ, normal to the triangle passing through the triangle's circumcenter; see Figure 9. In addition, the square grid angles formed by square grid edges incident to a square grid vertex in the folding can be no greater than 90° or the mapping would be expansive.

First, the mapping of any square grid angle incident to p approaches 0° as the square grid side length increases, with p placed ever further from the triangle along ℓ. Thus for some mapping of p onto ℓ, the maximum angle subtended by square grid edges at p in the folding can be made to equal 90°. Such a mapping of p is a locally non-expansive mapping of the square grid edges, and the distance between p and the triangle vertices under this mapping provides a lower bound on the length of a square grid edge.

Lastly, we must argue that square grid angles straddling two triangles, for example either square grid angle formed by vertices p, q, and a vertex adjacent to both, will also be nonexpansive. By definition of slowly varying, the angle between the two inward

pointing triangle normals of any two vertex adjacent triangles is always strictly less than 90°. As we increase the square grid edge length and p and q leave the surface along their respective normal lines, both square grid angles subtending p and q will approach some angle less than 90°. Then there exists a finite distance where these square grid angles are exactly 90°. This placement of p and q implies another lower bound on the length of a square grid edge. So we may set our square grid length according to the maximum, δ, over all lower bounds to produce a nonexpansive mapping of the square grid touching the target surface vertices. Because we have ensured that the square boundary grid maps to the surface nonexpansively, by [1], there exists an isometry of the individual squares that will fold to within distance δ to the target surface, which will be a δ-approximation of the target.

Now observe that δ must scale linearly with the maximum circumradius of any triangle in the triangulation. By refining the provided triangulation, we can scale the maximum circumradius arbitrarily small, thus for a given ε, we can refine the triangulation until δ is smaller than ε.

□

Figure 10 shows the simplest application of this construction to an equilateral triangular grid surface. Note that while this approximation can get arbitrarily close to the surface via triangle refinement, the efficiency of the construction, i.e. the ratio η/δ with η the length of the longest triangle edge of the target, will be unaffected by refinement. This construction can be extremely inefficient for triangulations containing triangles with large circumradius. We conjecture that there may be flexibility in the choice of refinement to bound the maximum circumradius, though we have not found such a refinement strategy. We also note that even local self-intersection can occur using this construction, so more work will be needed to apply this result to physical structures.

5.2 General 6-Regular

Now we describe a method to construct ε-approximations to general 6-regular triangulated orientable surfaces, where the dihedral angle between any two adjacent faces may be any value. Again, we will construct our approximation on one side of the surface, also containing the vertex set of the target surface.

Theorem 6. *Given a 6-regular triangulated surface, there exists a folding that is an ε-approximation to the surface for any positive value of ε.*

Proof. Unfortunately, the construction given for convex surfaces cannot be directly applied. In the slowly varying case, surface normals needed to be restricted to ensure that square grid angles straddling triangles could be made nonexpansive. However, when angles subtended by vertex adjacent triangles are less than 90° so that the angle between surface normals is *greater than* 90°, no such guarantee necessarily exists. We need to provide extra material between faces so that surface normals will be less constrained.

Thus we apply a slightly different association between square grid vertices and vertices of the triangulation: one that adds additional paper at triangle edges, mapping twelve square grid vertices to each vertex in the target triangulated surface instead of two; see Figure 11. We have added extra paper between every pair of adjacent faces, so an additional point, e.g. point q now resides on an edge between two triangles; see Figure 12. If we fix the folding of q to lie on the dihedral-angle-bisecting plane between the triangles, inward pointing triangle normals can be positioned without being constrained by direct adjacency. We can similarly place points locally similar to r along the average of the face normals from triangles sharing a square boundary with r.

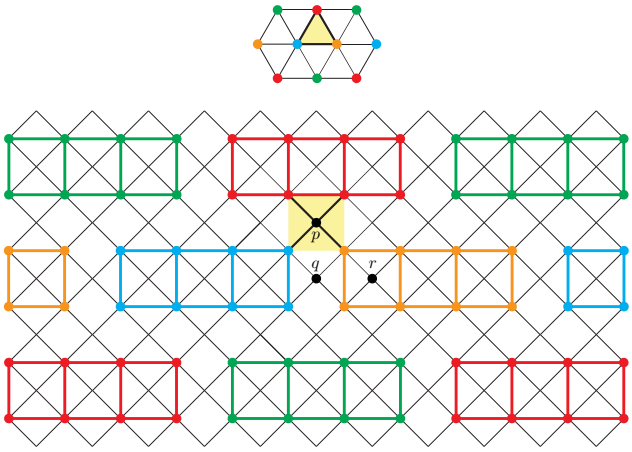

Fig. 11 Square grid to triangulation vertex correspondence for the general 6-regular construction. Twelve square grid vertices map onto each triangulated surface vertex. Point p is a square grid vertex associated with a face, q is associated with an edge, while r is associated with a vertex of the triangulation.

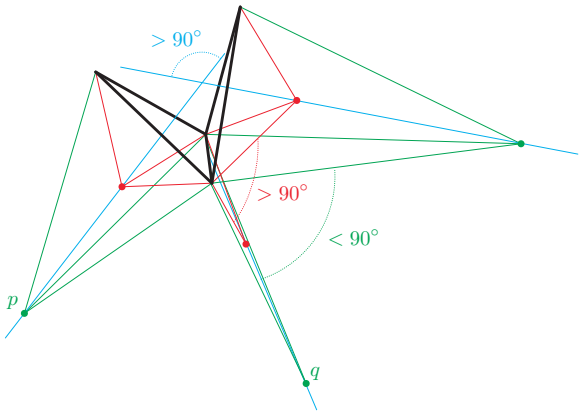

Fig. 12 Adding an additional edge vertex q between face vertices provides additional material necessary to accommodate face normals subtending angles larger than 90°.

Using the same strategy as in the slowly varying case, we can calculate finite lower bounds on square grid edge length from each angle and edge in the square grid, set our square grid edge length according to the maximum δ over all lower bounds, and fill in square boundary isometries for a δ-approximation of the target.

Again, δ must scale linearly with the maximum circumradius of any triangle in the triangulation, so we can scale the maximum circumradius arbitrarily small via refinement, and for a given ε, we can refine the triangulation until δ is smaller than ε.

□

Figure 13 shows this construction applied to an equilateral tri-

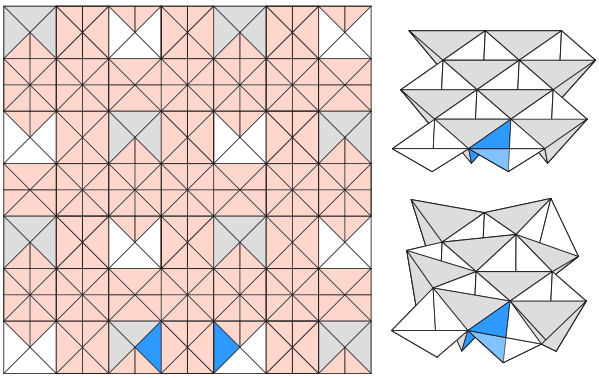

Fig. 13 A folding approximating an equilateral triangular grid using the general layout, and a contractive folding of the square boundaries to conform to a target triangulated surface. Isometries of the square interiors are not shown.

angular grid surface, and shortening edges of the grid to conform the mapping to a target triangulated surface, while keeping each square boundary of the grid contractive.

6. Conclusion

We have shown that crease patterns can be generated with foldings satisfying multiple prescribed boundary conditions, while folding finitely along all creases in the pattern. Our construction provides a method for designing for designing a single crease pattern that can approximate two different prescribed triangulated surfaces without self-intersection, by exploiting its modularity. Of course more study is needed to determine if variations of this construction can always construct an isometry that also avoids material self-intersection. If we want to produce universal transformable surfaces and programmable sheets of material, we will need to encourage the study of the kinds of surfaces discussed in this paper, seeking to produce not just a single folded form, but crease patterns that can adapt to many controllable designed states. We leave questions of satisfying more than two boundary conditions and avoiding self-intersection to future work.

References

[1] Erik D. Demaine and Jason S. Ku. Filling a hole in a crease pattern: Isometric mapping of a polygon given a folding of its boundary. In *Origami*^{6}*: Proceedings of the 6th International Meeting on Origami in Science, Mathematics and Education (OSME 2014)*, page to appear. Tokyo, Japan, August 10–13 2014.

[2] Robert J. Lang. A computational algorithm for origami design. In *Proc. 12th Symp. Computational Geometry*, pages 98–105, Philadelphia, PA, May 1996.

[3] Tomohiro Tachi. Generalization of rigid foldable quadrilateral mesh origami. In *Symposium of the International Association for Shell and Spatial Structures (50th. 2009. Valencia). Evolution and Trends in Design, Analysis and Construction of Shell and Spatial Structures: Proceedings*. Editorial Universitat Politècnica de València, 2009.

[4] Tomohiro Tachi. Origamizing polyhedral surfaces. *IEEE Transactions on Visualization and Computer Graphics*, 16(2):298–311, 2010.

Erik D. Demaine received a B.Sc. degree from Dalhousie University in 1995, and M.Math. and Ph.D. degrees from the University of Waterloo in 1996 and 2001, respectively. Since 2001, he has been a professor in computer science at the Massachusetts Institute of Technology. His research interests range throughout algorithms, from data structures for improving web searches to the geometry of understanding how proteins fold to the computational difficulty of playing games. In 2003, he received a MacArthur Fellowship as a "computational geometer tackling and solving difficult problems related to folding and bending moving readily between the theoretical and the playful, with a keen eye to revealing the former in the latter". He cowrote a book about the theory of folding, together with Joseph O'Rourke (Geometric Folding Algorithms, 2007), and a book about the computational complexity of games, together with Robert Hearn (Games, Puzzles, and Computation, 2009).

Jason S. Ku was born in 1986. Ku received Bachelor's, Master's, and Doctoral degrees in the Mechanical Engineering department at the Massachusetts Institute of Technology in 2009, 2011, and 2016 respectively. He now works there as a postdoctoral associate in computer science. He primarily studies computational geometry, particularly questions involving the relationship between two and three dimensions. His research topics include the design and fabrication of static and transformable folding structures from sheet-like material, 3D object reconstruction algorithms from lower dimensional projections, and 3D projection.

Appendix

Here we show that the locus of all satisfying single-vertex positions for a given nonexpansive folding of a simple quadrilateral is an ellipse. Consider a simple quadrilateral $abcd$ in the plane and a nonexpansive folding f of its boundary into $\mathbb{R}^3$. According to [1], there exists at least one point on the quadrilateral interior that defines a single-vertex crease pattern that folds to the boundary.

A point p is the vertex of a satisfying single-vertex crease pattern if there exists a point p_f in $\mathbb{R}^3$ such that $\|p-v\| = \|p_f - f(v)\|$ for all $v \in \{a, b, c, d\}$. Points p_f, $f(d)$, $f(a)$, and $f(b)$ define a tetrahedron in the folding. The approach will be to calculate p_f from p based on this tetrahedron, and then substitute into $\|p - c\| = \|p_f - f(c)\|$ to yield an equation in terms of the coordinates of p and the geometry of the input; see Figure A·1. We begin with the following manipulation:

$$\|p - c\| = \|p_f - f(c)\| \tag{A.1}$$

$$\|(p - a) - (c - a)\|^2 = \|(p_f - f(a)) - (f(c) - f(a))\|^2 \tag{A.2}$$

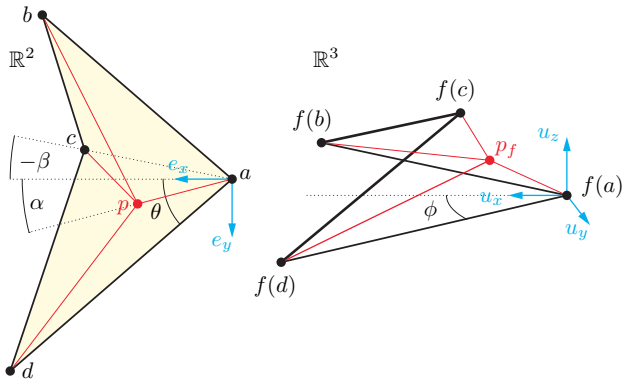

Fig. A·1 Geometry of a simple quadrilateral and a nonexpansive boundary folding f. Points p and p_f represent a candidate single vertex location to satisfy the boundary condition.

$$\begin{aligned}&\|p-a\|^2+\|c-a\|^2-2(p-a)\cdot(c-a)= \\ &\|p_f-f(a)\|^2+\|f(c)-f(a)\|^2-2(p_f-f(a))\cdot(f(c)-f(a)).\end{aligned} \tag{A.3}$$

Recall that $\|p-a\| = \|p_f-f(a)\|$, so letting $\lambda = \|c-a\|$ and $\lambda_f = \|f(c)-f(a)\|$ yields:

$$\lambda^2-\lambda_f^2-2(p-a)\cdot(c-a) = -2(p_f-f(a))\cdot(f(c)-f(a)) \tag{A.4}$$

Now we decompose these vectors in a convenient right-handed coordinate system. Let e_x be the unit vector in the plane parallel to the angle bisector of vertex a pointing locally interior to the polygon; let e_y be the unit vector in the plane perpendicular to e_x with positive dot product with $d-a$; and let $e_z = e_x \times e_y$. Let θ be the signed half angle of the interior angle at a defined by $e_x \times (d-a) = \|d-a\| \sin\theta\, e_z$; let α be the signed angle of $(p-a)$ relative to e_x defined by $e_x \times (p-a) = \|p-a\| \sin\alpha\, e_z$, and let β be the signed angle of $(c-a)$ relative to e_x defined by $e_x \times (c-a) = \|c-a\| \sin\beta\, e_z$. We will also parameterize p by its components in the e_x and e_y directions relative to a, so that $(p-a)\cdot e_x = \|p-a\|\cos\alpha = x$ and $(p-a)\cdot e_y = \|p-a\|\sin\alpha = y$. Then:

$$\begin{aligned}(p-a)\cdot(c-a) &= \|p-a\|\|c-a\|\cos(\alpha-\beta) \\ &= \lambda\|p-a\|(\cos\alpha\cos\beta+\sin\alpha\sin\beta) \\ &= d(x\cos\beta+y\sin\beta)\end{aligned} \tag{A.5}$$

Now we define a convenient right-handed coordinate system in folded space. Let u_x be a unit vector parallel to the angle bisector of angle $\angle f(d)f(a)f(b)$ with non-negative dot product with $f(b)-f(a)$; let u_y be the unit vector in the plane containing $f(d)$, $f(a)$, and $f(b)$, perpendicular to u_x with positive dot product with $f(c)-f(a)$; and let $u_z = u_x \times u_y$. Let ϕ be the signed angle defined by $u_x \times (f(d)-f(a)) = \|f(d)-f(a)\|\sin\phi\, u_z$. Then the components of $p_f - f(a)$ are given by:

$$\begin{aligned}&(p_f-f(a))\cdot u_x \\ &= (p_f-f(a))\cdot\frac{1}{2\cos\phi}\left(\frac{f(d)-f(a)}{\|f(d)-f(a)\|}+\frac{f(b)-f(a)}{\|f(b)-f(a)\|}\right) \\ &= (p-a)\cdot\frac{1}{2\cos\phi}\left(\frac{d-a}{\|d-a\|}+\frac{b-a}{\|b-a\|}\right) \\ &= \|p-a\|\frac{\cos(\theta-\alpha)+\cos(\theta+\alpha)}{2\cos\phi} \\ &= \|p-a\|\frac{\cos\theta\cos\alpha+\sin\theta\sin\alpha+\cos\theta\cos\alpha-\sin\theta\sin\alpha}{2\cos\phi} \\ &= \|p-a\|\frac{\cos\theta\cos\alpha}{\cos\phi} \\ &= x\frac{\cos\theta}{\cos\phi},\end{aligned} \tag{A.6}$$

$$\begin{aligned}&(p_f-f(a))\cdot u_y \\ &= (p_f-f(a))\cdot\frac{1}{2\sin\phi}\left(\frac{f(d)-f(a)}{\|f(d)-f(a)\|}-\frac{f(b)-f(a)}{\|f(b)-f(a)\|}\right) \\ &= (p-a)\cdot\frac{1}{2\sin\phi}\left(\frac{d-a}{\|d-a\|}-\frac{b-a}{\|b-a\|}\right) \\ &= \|p-a\|\frac{\cos(\theta-\alpha)-\cos(\theta+\alpha)}{2\sin\phi} \\ &= \|p-a\|\frac{\cos\theta\cos\alpha+\sin\theta\sin\alpha-\cos\theta\cos\alpha+\sin\theta\sin\alpha}{2\sin\phi} \\ &= \|p-a\|\frac{\sin\theta\sin\alpha}{\sin\phi} \\ &= y\frac{\sin\theta}{\sin\phi},\end{aligned} \tag{A.7}$$

and

$$\begin{aligned}(p_f-f(a))\cdot u_z &= \pm\sqrt{\|p-a\|^2-x^2\frac{\cos^2\theta}{\cos^2\phi}-y^2\frac{\sin^2\theta}{\sin^2\phi}} \\ &= \pm\sqrt{x^2\left(1-\frac{\cos^2\theta}{\cos^2\phi}\right)+y^2\left(1-\frac{\sin^2\theta}{\sin^2\phi}\right)}.\end{aligned} \tag{A.8}$$

The u_z component will be real only when $\|\alpha\| \le \|\phi\|$, which provides an immediate restriction on possible values of p; in particular, the magnitude of the angle α between $p-a$ and the angle bisector at a is bounded by $\phi \le \theta$. The equivalent angles at vertices b, c, d are similarly restricted, so satisfying p locations exist in and span the region bounded by these sectors; see the green region in Figure A·2. Letting $(f(c)-f(a))\cdot u_i = \lambda_i$ for $i \in \{x, y, z\}$ (such that $\lambda_f^2 = \lambda_x^2+\lambda_y^2+\lambda_z^2$), and substituting these intermediate results into equation A.4 yields:

$$\begin{aligned}&\frac{1}{2}(\lambda^2-\lambda_f^2)-\lambda(x\cos\beta+y\sin\beta)+x\frac{\cos\theta}{\cos\phi}\lambda_x+y\frac{\sin\theta}{\sin\phi}\lambda_y \\ &\qquad = \pm\sqrt{x^2\left(1-\frac{\cos^2\theta}{\cos^2\phi}\right)+y^2\left(1-\frac{\sin^2\theta}{\sin^2\phi}\right)}\lambda_z,\end{aligned} \tag{A.9}$$

which, after some rearrangement, yields the equation of a conic in the plane:

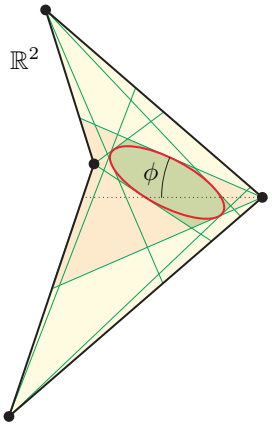

Fig. A·2 The locus of single vertex locations that satisfy the boundary condition is an ellipse that spans a symmetric angular region about the angle bisector at each vertex.

$$
\begin{aligned}
0 = {} & x^2\left(\left(\frac{\cos\theta}{\cos\phi}\,\lambda_x - \lambda\cos\beta\right)^2 - \left(1 - \frac{\cos^2\theta}{\cos^2\phi}\right)\lambda_z^2\right) \\
& + y^2\left(\left(\frac{\sin\theta}{\sin\phi}\,\lambda_y - \lambda\sin\beta\right)^2 - \left(1 - \frac{\sin^2\theta}{\sin^2\phi}\right)\lambda_z^2\right) \\
& + 2xy\left(\frac{\cos\theta}{\cos\phi}\,\lambda_x - \lambda\cos\beta\right)\left(\frac{\sin\theta}{\sin\phi}\,\lambda_y - \lambda\sin\beta\right) \\
& + 2x\left(\frac{\cos\theta}{\cos\phi}\,\lambda_x - \lambda\cos\beta\right)\frac{\lambda^2 - \lambda_f^2}{2} \\
& + 2y\left(\frac{\sin\theta}{\sin\phi}\,\lambda_y - \lambda\sin\beta\right)\frac{\lambda^2 - \lambda_f^2}{2} \\
& \left(\frac{\lambda^2 - \lambda_f^2}{2}\right)^2 . \qquad \text{(A.10)}
\end{aligned}
$$

As mentioned before, satisfying p locations are contained in a bounded region, so the conic defines an ellipse or circle. When the quadrilateral is a kite, $\lambda_y = (f(c) - f(a)) \cdot u_y = 0$ and $\sin\beta = 0$; the xy and y terms vanish, leaving an ellipse aligned with the diagonals, with center lying on the line of symmetry.